Finite-Element Analysis of Taylor Flow

Rolf K. Edvinsson and Said Irandoust

Dept. of Chemical Reaction Engineering, Chalmers University of Technology, S-412 96 Göteborg, Sweden

A finite-element analysis of Taylor flow in a cylindrical capillary was performed using a commercial FEM program (FIDAP) to solve the fundamental fluid dynamics equations together with the capillary forces at the gas–liquid interface. A moving-surface formulation was used to calculate the bubble shape. The thickness of the liquid film surrounding the gas bubble, the degree of mixing in the liquid phase, and the slip velocity between the two phases were calculated. These parameters influence the performance of monolith reactors operating in the Taylor flow regime. On comparison with experimental results it was found that the FEM calculation generally predicts a thinner liquid film, which can possibly be explained in terms of a peripheral variation in surface tension. Moreover, the wavelength of the wiggles predicted in the liquid film near the tail end of the bubble was compared to those arising from a simplified mathematical analysis available in the literature. Good agreement was found for $Ca < 0.005$, while for higher Ca the FEM predicts significantly shorter wavelengths, indicating that the lubrication theory is not valid here.

Introduction

Segmented gas–liquid flow, also known as Taylor flow, is an important flow pattern in cocurrent gas–liquid flow in monolithic catalyst reactors. A monolith consists of many narrow, parallel channels with the catalyst deposited on the walls. Monoliths are characterized by low-pressure drops and high surface-to-volume ratio. They are primarily used for gas–solid processes, but are also attractive for gas–liquid–solid reactions. The topic has been reviewed by Irandoust and Andersson (1988) and Cybulski and Moulijn (1994).

Taylor flow exhibits some special advantages for chemical processes. The gas bubble, having an equivalent diameter exceeding that of the capillary, is deformed into a long plug separated from the wall by only a very thin liquid film that permits high gas-to-wall mass-transfer rates. A recirculation pattern is induced in the liquid plug trapped between two gas plugs, which increases radial mass transfer and reduces axial dispersion.

Another example of two-phase flow of a wall-wetting liquid and a dispersed fluid in a capillary is found in enhanced oil recovery. Oil yield is increased by driving the oil from the porous rock by another fluid (a liquid or a foam). The rock

can be modeled as a network of narrow, cylindrical channels with a radius typically in the range $1–100$ μm (Schwartz et al., 1986). With low flow rates and narrow channels, capillary forces (surface tensional forces) dominate. As the channel diameter and flow rate are increased, viscous, inertial, and gravitational forces become influential as well. Flow regimes in gas–liquid flow are discussed by, among others, Taitel and Dukler (1976), Troniewski and Spisak (1987), and Whalley (1987).

Fairbrother and Stubbs (1935) pointed out that the liquid film surrounding the gas bubble caused the two phases to travel with slightly different speeds. This had implications for the practice of measuring liquid flow velocities by introducing an indicator bubble and measuring the speed of the latter. Their experiments led them to recommend the following correlation correcting for this difference: $1 - U_L/U_G = (\mu U_G/\gamma)^{1/2}$, where U_L and U_G denote the mean velocities of the liquid and gas phases. The group $\mu U/\gamma$ is a capillary number, Ca, and is the ratio between the viscous and the capillary forces (μ is the viscosity of the continuous, liquid phase). If nothing else is stated, the reference velocity, U, is the linear speed of the bubble. Their expression was valid in the range $10^{-3} < Ca < 10^{-2}$. Later, Taylor (1961) was able to extend this range to $10^{-3} < Ca < 10^{-1}$. If the film is thin, it is reasonable to assume that it is at rest with respect to the tube

Table 1. Correlations for Estimation of Liquid-Film Thickness

h_∞/R	Range	Method	Continuous Phase	Dispersed Phase	Reference
$0.5\,Ca^{1/2}$	$5\times10^{-5} < Ca < 3\times10^{-4}$	Conductimetry	Water	Air	Chen (1986)
$1.337\,Ca^{2/3}$	$2\times10^{-4} < Ca < 2\times10^{-3}$	Conductimetry	Water	Oil	Chen (1986)
$[0.89-0.05/(U_G)^{1/2}]\,Ca^{1/2}$ U_G in cm/s	$7\times10^{-6} < Ca < 2\times10^{-4}$	Conductimetry	Water, aqueous glycerol	Air, benzene	Marchessault and Mason (1960)
$1.337\,Ca^{2/3}$	$10^{-3} < Ca < 10^{-2}$	Volumetry	Aniline, benzene	Air	Bretherton (1961)
$0.36(1-\exp\{-3.08\,Ca^{0.54}\})$	$10^{-3} < Ca < 1.9$	Colorimetry	Water, ethanol, glycerol (aq)	Air	Irandoust and Andersson (1989b)
$0.5\,Ca^{1/2}$	$0.013 < Ca < 0.09$	Microscopy	Various oils	Various liquids	Goldsmith and Mason (1963)
$0.5\,Ca^{1/2}$	$10^{-3} < Ca < 10^{-2}$	Volumetry	Aniline, ethanol, benzene, water	Air	Fairbrother and Stubbs (1935)

wall, and then a simple mass-conservation argument leads to the following relationship:

$$1 - \frac{U_L}{U_G} = \frac{h_\infty}{R}\left(2 - \frac{h_\infty}{R}\right). \qquad (1)$$

Here h_∞ is the film thickness, measured far enough behind the bubble head to allow a film of constant thickness to develop, and R is the capillary radius. The relation between film thickness and capillary number has been investigated experimentally by several workers, as summarized in Table 1.

The mathematical analysis of Taylor flow is complicated by the fact that the bubble shape is part of the problem. At low Reynolds numbers it is justified to linearize the Navier–Stokes equations by the creeping flow assumption. It is, however, not sufficient to solve the equations of flow; the location of the boundary, or the shape of the domain, must be determined as well. Hence the overall problem remains nonlinear. By using additional simplifications, valid in the thin-film region, the problem can be reduced to a nonlinear ordinary differential equation (Bretherton, 1961). For high flow rates the assumption of potential flow has been used as a starting point for analyzing slug flow but, obviously, the problem of determining the bubble shape remains. For further details see Bendiksen (1985), Collins et al. (1978), Fabre and Liné (1992), Ginely and Radke (1989), Goldsmith and Mason (1963), Ratulowski and Chang (1990).

As an alternative to analytical methods, it is also possible to perform computational fluid dynamics simulations. A simple strategy is to solve the equations of flow for a fixed geometry and then adjust the shape on the basis of the solution in a second separate step. These two steps are then repeated until convergence is obtained. Irandoust and Andersson (1989a) and Mao and Dukler (1990) used the finite-difference method (FDM), while Shen and Udell (1985) and Westborg and Hassager (1989) used the finite-element method (FEM).

This decoupling of flow and shape, though simple, can cause convergence problems. A more sophisticated approach is to incorporate the location of the interface directly into the system of nonlinear equations arising from the equations of flow. One way to achieve this is to use the boundary integral equation method (Martinez and Udell, 1990; Stone and Leal, 1990).

In this work we examine the use of a FEM code to simulate Taylor flow over a wide range of flow conditions relevant to a monolithic catalyst reactor. The objectives are (1) to adapt a method that allows an accurate calculation of the flow pattern; (2) to derive performance characteristics from this solution; and (3) to establish, by a parameter study, the essential features of the relationship between, primarily, the film thickness and the various flow parameters.

Theory

Model assumptions

The model of Taylor flow, on which the subsequent development is built, is based on the following assumptions:

1. Equal size and spacing of the gas bubbles.
2. Periodicity of the velocity field in the axial direction.
3. The flow is steady in a coordinate system moving with a gas bubble. In a fixed coordinate system the flow would be nonstationary. In particular the boundary conditions at the channel inlet/outlet would be time-dependent.
4. The channel orientation is vertical with flow in either direction.
5. The flow is axially symmetric and nonswirling.
6. The flow is laminar, that is, the full Navier–Stokes equations are solved and no turbulence model is used.
7. Constant pressure within a gas plug. Also, the gas is assumed to have negligible density. This implies that the gas exerts a pressure on the liquid, but carries no momentum. This assumption allows us to remove the gas phase from the explicit calculation and greatly improves computational speed. This approach is also supported by work of Schwartz et al. (1986) and Westborg and Hassanger (1989).
8. All physical properties are considered to be constants, though the qualitative effect of a suspected variation in surface tension is given some attention.
9. The liquid plugs are long enough for a fully parabolic velocity profile to develop in the middle of them. This is not a necessary, but a convenient, assumption simplifying the formulation of the boundary conditions.

Governing equations

The equations of flow and the necessary boundary conditions given in the following sections are all presented in the dimensionless form. Details are given in the Notation section and Figure 1. Conservation of momentum in the radial and axial directions:

$$u_r\frac{\partial u_r}{\partial r} + u_z\frac{\partial u_r}{\partial z} = \frac{1}{r}\frac{\partial}{\partial r}(r\sigma_{rr}) - \frac{1}{r}\sigma_{\theta\theta} + \frac{\partial \sigma_{rz}}{\partial z} \qquad (2)$$
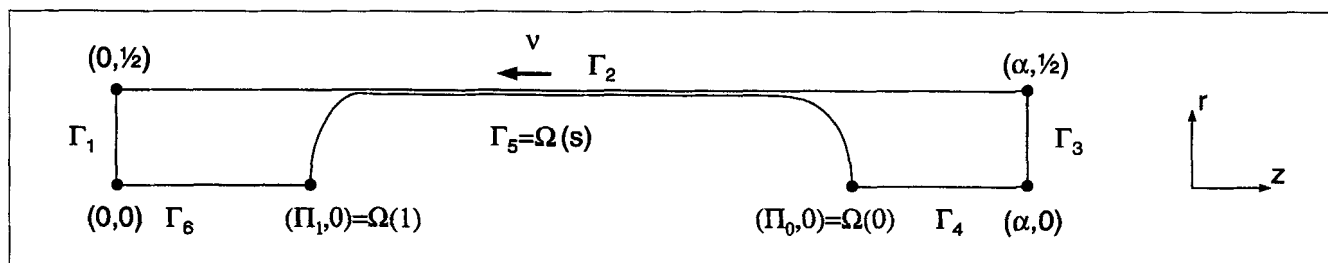
Figure 1. Geometry of the computational domain.

$$u_r \frac{\partial u_z}{\partial r} + u_z \frac{\partial u_z}{\partial z} = \frac{1}{r} \frac{\partial}{\partial r}(r\sigma_{rz}) + \frac{\partial \sigma_{zz}}{\partial z} + \frac{1}{Fr}. \tag{3}$$

This can be made to be applied to both upward and downward flow if we assume that the direction of flow is the positive z-direction and use the convention that $Fr > 0$ corresponds to downward flow and $Fr < 0$ signifies upward flow. The various stresses that appear in Eqs. 2 and 3 are given by the following expressions:

$$\sigma_{rr} = -p + \frac{2}{Re} \frac{\partial u_r}{\partial r}; \qquad \sigma_{\theta\theta} = -p + \frac{2}{Re} \frac{u_r}{r};$$

$$\sigma_{rz} = \frac{1}{Re}\left(\frac{\partial u_r}{\partial z} + \frac{\partial u_z}{\partial r}\right); \qquad \sigma_{zz} = -p + \frac{2}{Re} \frac{\partial u_z}{\partial z}. \tag{4}$$

The continuity equation:

$$\frac{1}{r} \frac{\partial}{\partial r}(r u_r) + \frac{\partial u_z}{\partial z} = 0. \tag{5}$$

Boundary conditions

The equations are solved with reference to a translating coordinate system. The constant rate of translation is $v > 0$. A parabolic velocity profile is imposed at the end of the computational system, that is, on the boundary segment Γ_3 (see Figure 1)

$$u_z|_{\Gamma_1} = u_z|_{\Gamma_3} = 2(1 - 4r^2) - v, \tag{6}$$

and the periodic velocity condition is

$$u_r|_{\Gamma_1} = u_r|_{\Gamma_3}. \tag{7}$$

At the wall:

$$u_r|_{\Gamma_2} = 0; \qquad u_z|_{\Gamma_2} = -v. \tag{8}$$

Axial symmetry:

$$u_r|_{\Gamma_4} = u_r|_{\Gamma_6} = 0; \qquad \frac{\partial u_z}{\partial r}\bigg|_{\Gamma_4} = \frac{\partial u_z}{\partial r}\bigg|_{\Gamma_6} = 0. \tag{9}$$

Since we assume that the bubble possesses rotational symmetry, it suffices to use a single curve to represent its shape. The interface between the gas and the liquid, Γ_5, can thus be

considered to be a mapping of the interval $[0,1]$ onto the $r - z$ plane:

$$\Gamma_5 = \Omega(s) \qquad 0 \le s \le 1. \tag{10}$$

At the gas–liquid interface

$$\frac{\partial u_t}{\partial n}\bigg|_{\Gamma_5} = -\nabla \gamma, \tag{11}$$

and the righthand side of this expression reduces to zero when variations in surface tension are neglected. A stable gas plug moving with the same speed as the coordinate system, v, must obey the following condition in order to retain its shape and position:

$$u_n|_{\Gamma_5} = 0. \tag{12}$$

The endpoints of the curve defining the interface must, due to symmetry considerations, intersect the axis of symmetry at a right angle.

Since we are considering incompressible fluids the pressure level can be selected arbitrarily. With the gas side pressure set to zero, the stress balance at the curved interface relates the curvature of the interface to the liquid side pressure:

$$p|_{\Gamma_5} = -\frac{2}{ReCa}H + \frac{2}{Re} \frac{\partial u_n}{\partial n}. \tag{13}$$

The boundary conditions on the liquid-phase velocities are such that liquid volume is conserved. Since the system volume is constant, the gas volume is also conserved.

Nondimensional parameters

The linear velocity of the bubble is frequently used as a reference velocity but, since it is treated as a dependent variable in this work, it is more convenient to use the mean velocity of the two phases as the reference velocity:

$$\langle U \rangle = \frac{4}{\pi}\left(\frac{Q_G + Q_L}{D^2}\right). \tag{14}$$

With the channel diameter, D, as the characteristic length, the unit of time becomes $D/\langle U \rangle$, the time required to move a distance D at the average velocity. To completely charac-
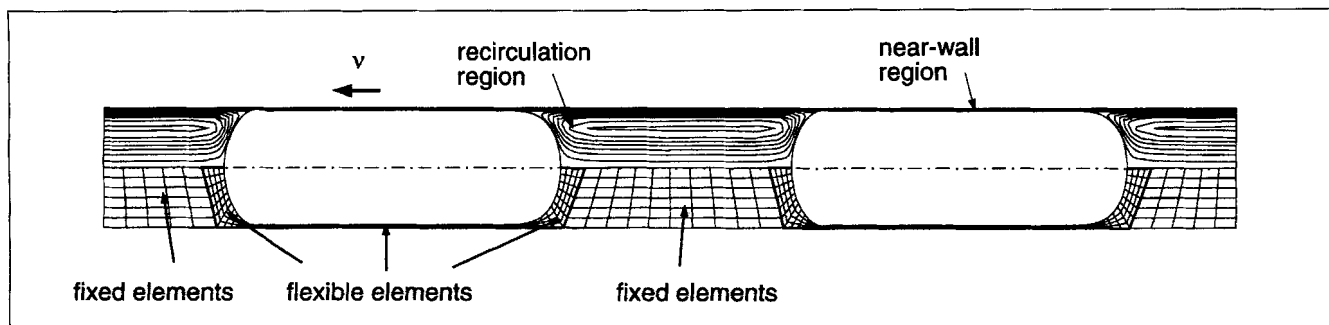
Figure 2. Final mesh and the corresponding streamlines.

terize the system, five dimensionless groups are needed. They are the Reynolds, Froude, and capillary groups

$$Re = \frac{D\rho\langle U \rangle}{\mu} \qquad Fr = \frac{\langle U \rangle^2}{gD} \qquad Ca = \frac{\mu\langle U \rangle}{\gamma}, \quad (15)$$

as well as the void fraction, ϵ, and the aspect ratio, α:

$$\epsilon = \frac{V_G}{V_G + V_L} \qquad \alpha = \frac{L_p}{D}. \quad (16)$$

Finite-Element Simulation

Discretization

The meshing of the domain is also illustrated in Figure 2. Nine node quadrilateral elements have been used. Two types of elements have been employed; those filling the region surrounding the bubble are flexible and may change their shapes and sizes in order to accommodate the motion of the interface, while the rest are fixed in space. The interface must lie inside the region of flexible elements. Moreover, each node is constrained to a prespecified line, denoted a spine. For further details see FIDAP, Theoretical Manual (1991).

Solution strategy

The mathematical problem is composed of several parts. The conservation equations apply in the fluid phase, a two-dimensional domain. The bubble shape is described by a curve and thus has a one-dimensional domain. Finally, the (scalar) speed of the gas plug is a dependent variable. To illustrate this we may represent the problem that we set out to solve by a function f_1:

$$(\nu, \delta_f) = f_1(Re, Fr, Ca, \epsilon, \alpha). \quad (17)$$

Unfortunately this problem cannot easily be solved in a single-step simulation with the present simulation. This is because the boundary conditions are functions of the bubble speed, which we do not know beforehand. Two approaches are possible. First we may vary the translational speed of our coordinate system so that it matches the bubble speed. This will require inclusion of acceleration terms, since the coordinate system is not moving with constant speed. The alternative approach, used in this work, is to temporarily drop the

requirement that the bubble should remain at the same position. This leads to the following nonstationary problem, represented by a function f_2:

$$(\nu'', \delta_f) = f_2(Re, Fr, Ca, \epsilon, \alpha, \nu') \quad (18)$$

Here ν' is the currently best estimate of the bubble velocity, which is identical to the translational speed of the coordinate system. The bubble is now free to move, and the net drift velocity is the difference between the actual velocity and the translation velocity of the coordinate system:

$$\nu'' = \nu - \nu'. \quad (19)$$

Now ν is determined iteratively by finding the value of ν that makes the drift velocity zero, that is, ν is selected so that the boundary condition (Eq. 12) is satisfied. In practice, a transient solution is obtained for a short time period based on a first guess of the drift velocity. The observed drift velocity is then used to adjust this value. This procedure normally converges rapidly, after which it is possible to perform a long transient simulation with virtually no change in bubble shape and position. In most runs, this technique was used to pin down the velocity to four or five decimal places. It should be pointed out that if a steady-state simulation is attempted, even the slightest error in the estimate of ν would cause a net drift. As the interface reaches the limit of the flexible elements, mesh destruction is inevitable.

Another problem, related to the formulation of the boundary conditions, is how to drive the liquid through the channel. It would be desirable to impose a finite pressure drop over a long section encompassing many bubbles. This would be computationally demanding, and in the present work we have restricted ourselves to one repetitive unit. Three formulations of the boundary conditions have been tried: (1) imposing a pressure drop across one gas/liquid unit; (2) imposing a parabolic; and (3) a flat axial velocity profile on Γ_1 and Γ_3. All formulations gave very similar results. The Parabolic profile is used henceforth since it is both convenient and realistic.

Results and Discussion

A typical shape of a Taylor bubble is shown in Figure 3a. The plot of streamlines indicates the surrounding flow field. It can be seen that the liquid phase can be divided into two
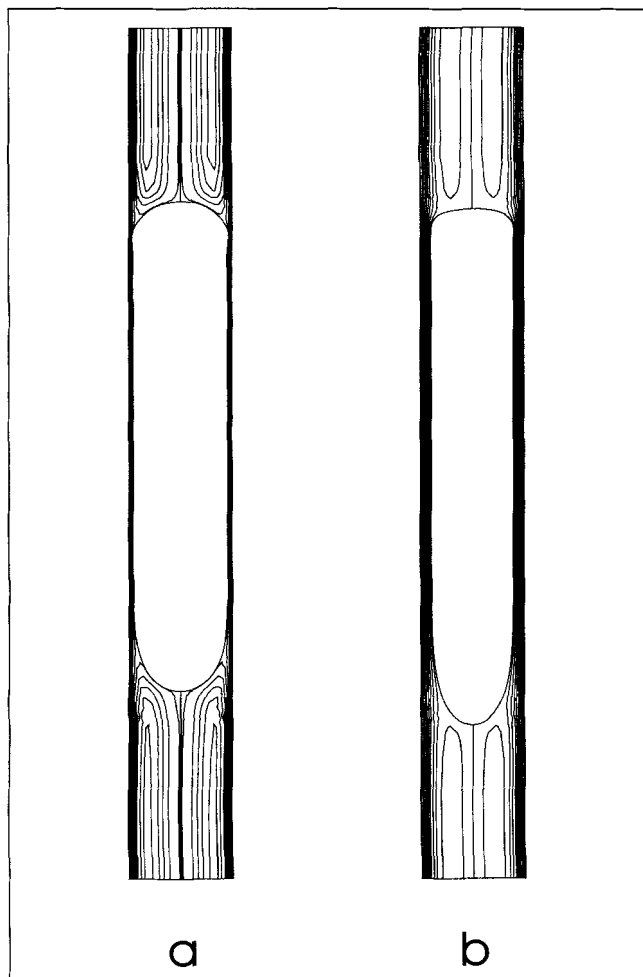
**Figure 3. Effect of viscosity ($\mu_b = 5\mu_a$) on the stream-
line pattern.**

(a) $Re = 100$, $Fr = 1$, $Ca = 0.04$, $\alpha = 8$, $\epsilon = 0.50$. (b) $Re = 20$,
$Fr = 1$, $Ca = 0.04$, $\alpha = 8$, $\epsilon = 0.50$.

regions. The closed streamlines within the liquid plug form a
recirculation region, and the open-ended streamlines passing
through the liquid film mark liquid elements that will remain
in the vicinity of the wall. Increasing the viscosity by a factor
of 5 results in the situation illustrated in Figure 3b. The bub-
ble head is more pointed and the tail almost flat. In addition,
a much thicker film is formed and the recirculation is signifi-
cantly reduced.

Solution accuracy

When assessing the quality of the numerical solution, two
kinds of questions need to be addressed: (1) Is this an accept-
ably converged solution to the set of equations we wanted to
solve? and (2) Are the assumptions made in order to obtain
this set of equations acceptable? The latter question can be
represented by the artificial boundary conditions that must
be applied in order to limit the size of the computational
domain. Ideally we would like these assumptions to be neu-
tral in the sense that they do not significantly affect the im-
portant aspect of the resulting solution.

At both ends of the computational system, approximately
in the center of the liquid plug, a parabolic velocity profile
was prescribed. As a test, a flat velocity profile, giving the
same volumetric flow rate as the parabolic one, was imposed
instead. The effect on the film thickness, and thus ν, was
minor, even when the liquid plug length was about one capil-
lary diameter. Similarly, the length of the gas plug had no
effect as long as it was large enough to form a plug.

The proper convergence of the solution was tested in sev-
eral ways. The nodal density of the mesh was varied in order
to establish grid independence. Since a transient solution
method was used only as a means to obtain a steady-state
solution, a relatively high tolerance was used. As a steady-
state solution appeared to have been reached, the tolerance
could be reduced by five orders of magnitude without signifi-
cantly altering the solution. Before the bubble had relaxed to
its final shape, the time increment was limited by stability
considerations; as the final shape was reached this limit in-
creased, sometimes permitting a single time step of 20 to be
taken. This corresponds to the bubble moving a length of ap-
proximately 20 diameters in one step without changing shape,
and implies that a steady-state solution of high quality was
obtained. In most cases, a solution could be obtained within
5 to 30 CPU minutes using a HP720 workstation, provided
that a good starting guess was supplied. In many cases the
procedure had to be repeated a few times to allow revision of
meshing.

The calculation of wiggles, especially when the inertial
forces were significant, was more demanding. In order to re-
solve the wiggles a finer mesh was employed; moreover, a
small time increment was required to maintain stability. As a
result, some of these calculations required 10 CPU hours or
more.

Influence of the capillary number

Figure 4a–4d constitutes a sequence illustrating what hap-
pens when the viscous effects become more dominant. The
parameters of Figure 4 are given in Table 2. The convexity of
the rear meniscus is first lost and then finally inverted. If the
diameter is sufficiently large and the liquid viscous enough, it
is possible for the inverted rear meniscus to penetrate all the
way through the bubble. This can under some circumstances
result in a stable toroidal bubble. This peculiar flow pattern
is called *stalactite flow* (Edvinsson et al., 1992).

The effect of inertial forces

In reaction engineering applications, we can expect to en-
counter higher flow rates than those typical of capillary flows.
As the Re number increases, the almost perfectly spherical
ends typical of the flow dominated by capillary forces are lost.
The sequence in Figures 4e–4g, corresponding to Reynolds
numbers 500, 1,000, and 2,000, illustrates this. In the film
near the rear meniscus, a multiple wavelet has formed and its
amplitude increases with Re. The film is also predicted to
thicken slightly, though a precise measure is difficult since
there no longer appears to be a region of constant thickness.
This sequence also represents increasing computational diffi-
culties; as the critical Re number is approached, one needs
to shorten the time steps in order to achieve convergence at
all. Therefore the cautious reader should consider the shapes
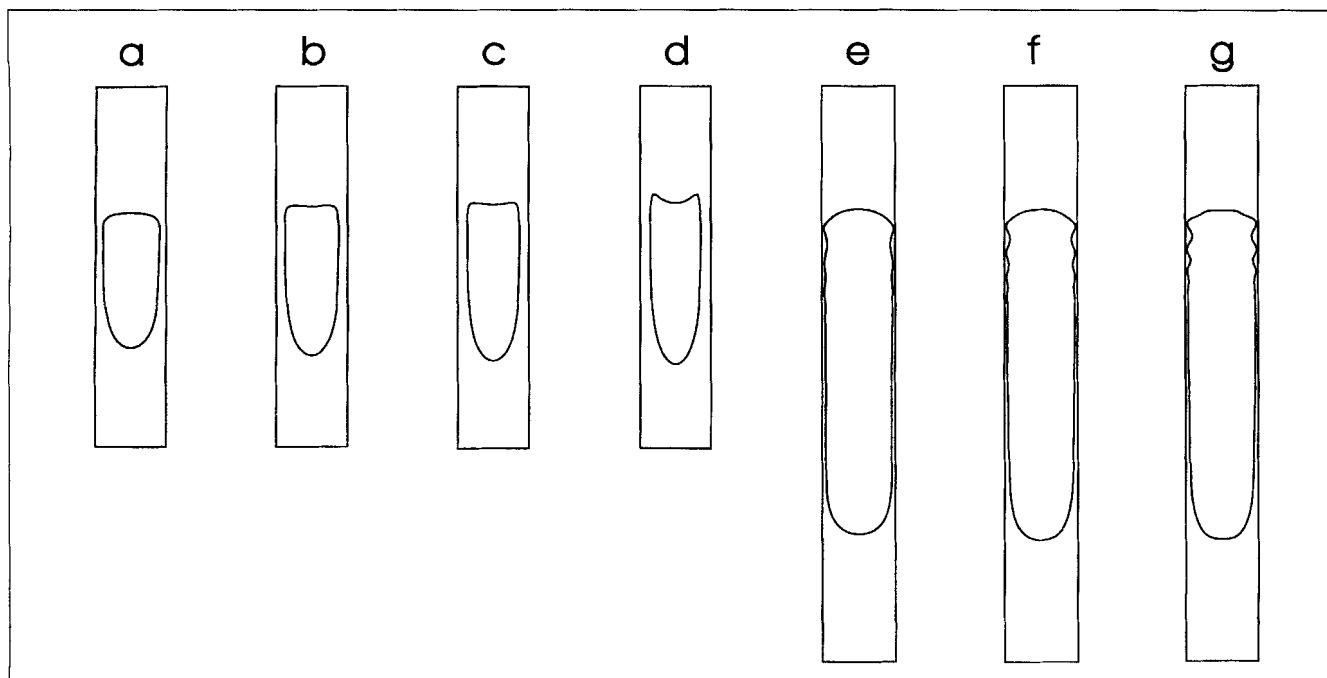
Figure 4. Calculated bubble shapes.

The parameters are summarized in Table 2.

in Figures 4e–4g as "snapshots" rather than steady-state solutions, since it cannot be guaranteed that the solution is fully converged. Indeed, an oscillating solution is encountered.

Undulations in the liquid film

Wiggles, very similar to the ones calculated here, have been observed experimentally (Figure 5). As their amplitudes are increased still further, a snap-off process can occur in which the bubble splits into two smaller ones in close proximity.

Ratulowski and Chang (1989) used an arclength formulation of the lubrication equations to calculate the bubble profiles. After some simplifications, their analysis led to an analytical expression for the characteristic wavelength, which in our notation becomes
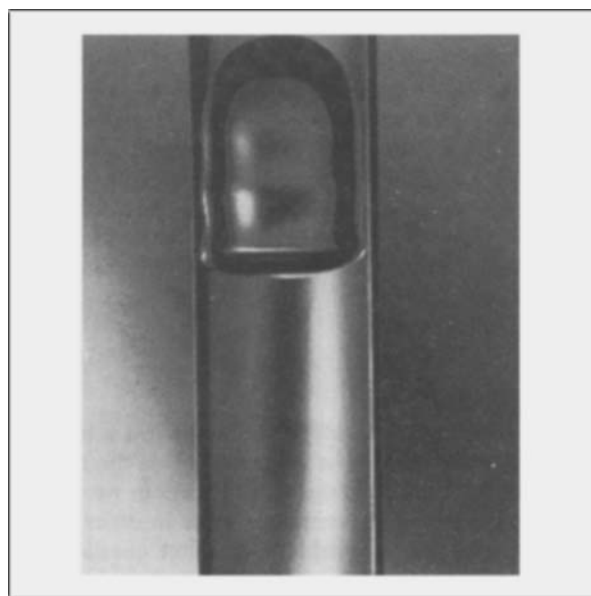
$$\lambda = \frac{2\pi}{\sqrt{3}\,(\beta_1^{1/3} - \beta_2^{1/3})},\qquad(20)$$

where

$$\beta_{1,2} = \frac{Ca_b\gamma}{2} \pm \sqrt{\left(\frac{Ca_b\gamma}{2}\right)^2 + \frac{1}{27r_0^6}}\ ;\quad Ca_b = Ca\,v\ ;$$

$$\gamma = \frac{32r_0}{4r_0^4 \ln r_0 - 3r_0^4 + 4r_0^2 - 1}.\qquad(21)$$

Table 2. Parameters Used in the Simulations in Figure 4

Label	α	ϵ	Re	$1/Fr$	Ca
a	5	0.2	20	1.0	0.20
b	5	0.2	20	1.0	0.38
c	5	0.2	20	1.0	0.50
d	5	0.2	20	1.0	1.0
e	8	0.5	500	0	0.01
f	8	0.5	1,000	0	0.01
g	8	0.5	2,000	0	0.01

Figure 5. Undulations in the liquid film.

Petroleum ether and air at 20°C in a glass capillary of internal diameter 4.3 mm. Flow rates: petroleum ether 0.523 mL/s, air 0.023 mL/s (upflow).
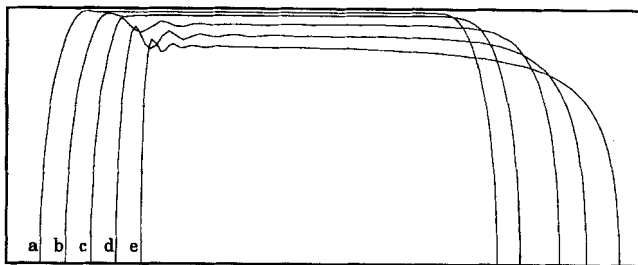
Figure 6. Shapes of Taylor bubbles as a function of the capillary number.

Ca is (a) 0.001; (b) 0.0032; (c) 0.01; (d) 0.03; and (e) 0.06.

The value of r_0 can be evaluated by using Bretherton's limit

$$r_0 = 1 - 1.3375\,Ca_b^{2/3}. \tag{22}$$

As an illustration consider the bubble profiles shown in Figure 6. The capillary number, and thus the film thickness, increase in the sequence a–e (note that the aspect ratio has been changed to highlight the wiggles).

It is possible to estimate the wavelengths from Figure 6 even though the undulations are not perfect sine waves. We see that initially both the amplitude and the wavelength go through a maximum on increasing *Ca*. The estimated wavelengths are plotted in Figure 7. In addition the analytical prediction (Eqs. 20–22) is plotted. The middle curve was obtained by using the r_0 from the FEM calculation rather than the Bretherton limit of Eq. 22. The discrepancy between the two predictions is reduced, though the maximum found in the FEM calculation is not predicted. This suggests that the lubrication theory is acceptable up to a *Ca* of about 0.005. A possible explanation for the different behavior at higher *Ca* is that the bubble becomes unsteady.
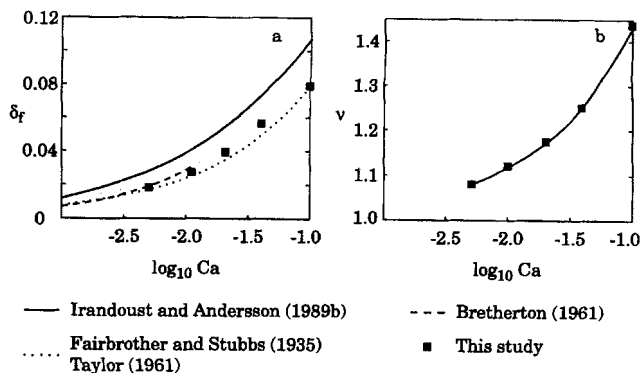
Parameter study

The dependence of the film thickness, δ_f, and the relative velocity of the gas plug, ν, on a number of parameters has been studied. The focus has been on the *Re*, *Fr*, and *Ca* groups since the aspect ratio, α, and the void fraction, ϵ, are found to be relatively unimportant in the region of interest. As long as the gas bubble is large enough to allow a distinct film region to develop, any change in its volume will affect only the bubble length, not the film thickness and the flow rate.
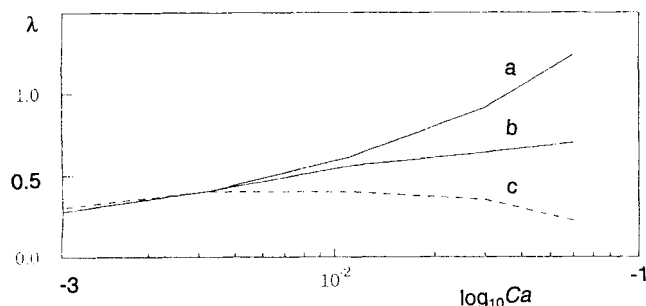
Figure 7. Wavelengths near tail.

(a) Predicted by Eqs. 20–22; (b) as case *a*, but r_0 is taken from the FEM simulation; (c) FEM simulation.

—— Irandoust and Andersson (1989b)   – – – Bretherton (1961)

..... Fairbrother and Stubbs (1935)   ■ This study
Taylor (1961)

Figure 8. Influence of *Ca* on (a) δ_f; (b) ν.

$Re = 200$, $\alpha = 8$, $\epsilon = 0.5$, $Fr^{-1} = 0$.

For small capillaries it is sufficient to correlate the film thickness and the relative velocity with the *Ca* number. As flow rates and diameters are increased, the influences of inertial forces as well as gravitational forces become more pronounced. The dependence of δ_f and ν on *Ca* is illustrated in Figure 8. Gravitational forces have been omitted here. Superimposed are the results of some other workers. The overall behavior is the same, though the FEM solution systematically predicts thinner liquid films than those reported experimentally (see Table 1).

The influence of gravity is illustrated in Figure 9. The reciprocal of the Froude group is proportional to the gravitational acceleration. A negative sign represents upflow. For low *Ca* numbers, the film is thin and only a small velocity gradient develops in the film. As the film becomes thicker, substantial deviations from the assumption of a stagnant film occur. The strongest effect is found in upward flow.

Based on the sequence in Figures 4e–4g, we note that there appears to be a dependence of the film thickness on the *Re* number as well. As *Re* increases the film becomes thicker, and the slip velocity between the two phases increases. As long as the flow is laminar, the effect is rather small and, due to the problems of ensuring that this is a converged solution, no attempt was made to quantify it.

There are a few possible explanations for the discrepancy between the film thicknesses predicted by the simulation and those measured experimentally. The correlation of Irandoust and Andersson (1989b) was based on measurements of light absorption. In order to minimize the distance the light has to travel through the liquid film, it must follow a line that passes through the centerline of the capillary. If the focus is slightly
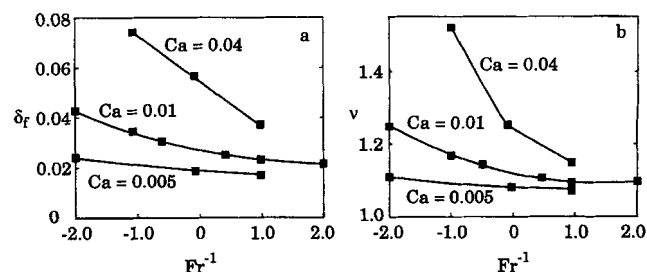
Figure 9. Influence of Fr^{-1} on (a) δ_f; (b) ν.

$Re = 200$, $\alpha = 8$, $\epsilon = 0.5$.
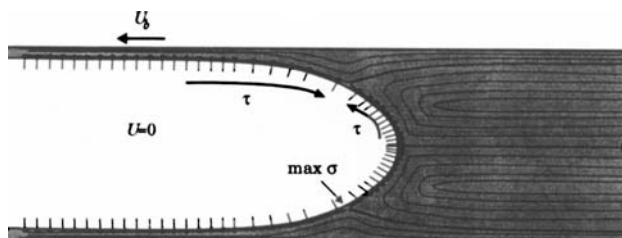
Figure 10. Buildup of surface tension gradients through the adsorption of surfactants.

off, or the light beam passes through an area rather than a point, the result will be an overprediction of the film thickness. The calculated thickness, on the other hand, represents the result of a perfect reading, and is thus the smallest value that would be observable for real flow.

The influence of a variable surface tension can also explain a similar discrepancy. In a system with very pure liquid, the assumption of constant surface tension is likely to be correct; however, such systems are not likely to be found outside the laboratory. As a small portion of liquid, containing trace amounts of surface-active impurities, is brought to the interface, these impurities start to accumulate at the interface. As the surface concentration increases, the interfacial tension is reduced. Hence the surface tension changes with age. A variation of the surface tension leads to a tangential force at the interface in the direction from low to high surface tension.

This effect explains the significantly higher rise velocity of an air bubble in very pure water compared to water of ordinary purity (Clift et al., 1978). The fresh liquid is exposed to the gas at the top of the bubble, and as it moves along the periphery surfactants accumulate, surface tension drops, and a force, opposing the motion, results.

In the case of a Taylor bubble, the situation is a bit more complicated. The fresh liquid now reaches the interface at the stagnation ring, rather than at the top, and is there divided into two streams (see Figure 10). Hence the surface tension will have its maximum value at the stagnation ring, and a gradient will form on both sides. In the film this gradient will give rise to a tangential force that tends to drain liquid from the film, thus making it thinner. In front of the stagnation ring, the gradient gives rise to a tangential force acting in the opposite direction and thus increasing the film thickness. The rate at which the surface tension drops from the value of the fresh liquid/gas interface is a complicated function of the bulk concentration and distribution of impurities, their effective diffusivity, the adsorption isotherm at the interface, and the relationship between surface concentration and surface tension.

Conclusions

It has been shown that a commercial software package can be used to analyze the flow of a Taylor bubble in a capillary under a wide range of conditions. The approach taken here allows the simultaneous inclusion of viscous, gravitational, inertial, and capillary forces into the model. The bubble shape and the velocity field in the liquid phase are obtained from the simulations. The predicted thicknesses of the liquid film surrounding the gas bubble were slightly lower than those

observed experimentally by Irandoust and Andersson (1989b). The influence of the Reynolds number was found to be small in the laminar regime. The influence of gravitational forces was also studied and was found to be significant for high Ca and upflow. For $Ca < 0.01$ and $Fr < 1$, this effect is small. The size of the recirculation cell within the liquid plug was found to decrease rapidly with increasing film thickness.

Predictions of the undulations occurring in the liquid film, predominantly near the tail end, were compared to an analysis using lubrication theory by Ratulowski and Chang (1989). Agreement was good for $Ca < 0.005$, while the FEM predicted shorter wavelengths at higher Ca. The behavior of the FEM solution indicates that the oscillations become unstable for higher Ca, suggesting that the lubrication theory no longer applies.

Notation

g = gravitational acceleration, m/s^2
H = mean Gaussian curvature
L_p = period length (gas + liquid plug), m
n = normal direction
p = pressure
Q = flow rate, m^3/s
$r = R/D$, radial coordinate
r_0 = bubble radius
s = dummy variable introduced in Eq 10
t = tangential direction
$\langle U \rangle$ = total mean linear velocity, m/s
u = velocity component
V = volume of the gas phase in the computational domain, m^3
z = axial coordinate

Greek letters

β_i = parameter defined by Eq. 21
γ = surface tension, N/m; parameter defined by Eq. 21
θ = angular direction
λ = characteristic wavelength
Π = anchor point of interface (Figure 1)
ρ = density of liquid, kg/m^3
σ = stress
Ω = function describing bubble shape

Literature Cited

Bendiksen, K. H., "On the Motion of Long Bubbles in Vertical Tubes," *Int. J. Multiphase Flow*, **11**(6), 797 (1985).

Bretherton, F. P., "The Motion of Long Bubbles in Tubes," *J. Fluid Mech.*, **10**, 166 (1961).

Chen, J.-D., "Measuring the Film Thickness Surrounding a Bubble inside a Capillary," *J. Colloid Interf. Sci.*, **109**(2), 341 (1986).

Clift, R., J. R. Grace, and M. E. Weber, *Bubbles, Drops, and Particles*, Academic Press, New York (1978).

Collins, R., F. F. de Moraes, J. F. Davidson, and D. Harrison, "The Motion of a Large Gas Bubble Rising through Liquid Flowing in a Tube," *J. Fluid Mech.*, **89**(3), 497 (1978).

Cybulski, A., and J. A. Moulijn, "Monoliths in Heterogeneous Catalysis," *Cat. Rev. Sci. Eng.*, **36**(2), 179 (1994).

Edvinsson, R., R. Sandboge, S. Irandoust, and W. Spisak, "The Stalactite Flow of a Gas-Viscous Liquid in Vertical Tubes," *Adv. Finite Elem. Anal. Fluid Dyn., FED*, **137**, 107 (1992).

Fabre, J., and A. Liné, "Modeling of Two-Phase Slug Flow," *Ann. Rev. Fluid Mech.*, **24**, 21 (1992).

Fairbrother, F., and A. E. Stubbs, "Studies in Electro-endosmosis. Part VI: The 'Bubble-tube' Method of Measurement," *Chem. Soc.*, **1**, 527 (1935).

FIDAP, *Fluid Dynamics Analysis Package*, Fluid Dynamics International, Inc., Evanston, IL 60201 (1991).

Ginely, G. M., and C. J. Radke, "Influence of Soluble Surfactants on the Flow of Long Bubbles through a Cylindrical Capillary," *ACS Symp. Ser.*, **396**, 480 (1989).

Goldsmith, H. L., and S. G. Mason, "The Flow of Suspensions through Tubes. II: Single Large Bubbles," *J. Colloid Sci.*, **18**, 237 (1963).

Irandoust, S., and B. Andersson, "Monolithic Catalysts for Nonautomobile Applications," *Cat. Rev. Sci. Eng.*, **30**(3), 341 (1988).

Irandoust, S., and B. Andersson, "Simulation of Flow and Mass Transfer in Taylor Flow through a Capillary," *Computers Chem. Eng.*, **13**(4/5), 519 (1989a).

Irandoust, S., and B. Andersson, "Liquid Film in Taylor Flow through a Capillary," *Ind. Eng. Chem. Res.*, **28**(11), 1684 (1989b).

Mao, Z.-S., and A. E. Dukler, "The Motion of Taylor Bubbles in Vertical Tubes: I. A Numerical Simulation for the Shape and Rise Velocity of Taylor Bubbles in Stagnant and Flowing Liquid," *J. Comput. Phys.*, **91**, 132 (1990).

Marchessault, R. N., and S. G. Mason, "Flow of Entrapped Bubbles through a Capillary," *Ind. Eng. Chem.*, **52**(1), 79 (1960).

Martinez, M. J., and K. S. Udell, "Axisymmetric Creeping Motion of Drops Through Circular Tubes," *J. Fluid Mech.*, **210**, 565 (1990).

Ratulowski, J., and H.-C. Chang, "Transport of Gas Bubbles in Capillaries," *Phys. Fluids A1*, **10**, 1642 (1989).

Ratulowski, J., and H.-C. Chang, "Marangoni Effects of Trace Impurities on the Motion of Long Gas Bubbles in Capillaries," *J. Fluid Mech.*, **210**, 303 (1990).

Schwartz, L. W., H. M. Princen, and A. D. Kiss, "On the Motion of Bubbles in Capillary Tubes," *J. Fluid Mech.*, **172**, 259 (1986).

Shen, E. I., and K. S. Udell, "A Finite Element Study of Low Reynolds Number Two-Phase Flow in Cylindrical Tubes," *J. Appl. Mech.*, **52**, 253 (1985).

Stone, H. A., and L. G. Leal, "The Effects of Surfactants on Drop Deformation and Breakup," *J. Fluid Mech.*, **220**, 161 (1990).

Taitel, Y., and A. E. Dukler, "A Model for Predicting Flow Regime Transitions in Horizontal and Near Horizontal Gas-Liquid Flow," *AIChE J.*, **22**, 47 (1976).

Taylor, G. I., "Deposition of a Viscous Fluid on the Wall of a Tube," *J. Fluid Mech.*, **10**, 161 (1961).

Troniewski, L., and W. Spisak, "Flow Patterns in Two-Phase Downflow of Gas and Viscous Liquid," *Int. J. Multiphase Flow*, **13**, 257 (1987).

Westborg, H., and O. Hassager, "Creeping Motion of Long Bubbles and Drops in Capillary Tubes," *J. Colloid Interf. Sci.*, **133**(1), 135 (1989).

Whalley, P. B., *Boiling, Condensation and Gas-Liquid Flow*, Clarendon Press, Oxford (1987).